

1 **Title: Nanomicelles potentiate histone deacetylase inhibitor efficacy in vitro.**

2  
3 **S. Pisano<sup>\*12</sup>, X. Wang<sup>\*345</sup>, J. Garcia Parra<sup>1</sup>, A. Gazze<sup>1</sup>, K. Edwards<sup>1</sup>, V. Feltracco<sup>1</sup>, Y. Hu<sup>34</sup>, L. He<sup>4</sup>, D. Gonzalez<sup>1</sup>, L.W. Francis<sup>1</sup>, R.S. Conlan<sup>1</sup>, C. Li<sup>4\*\*</sup>**

4  
5  
6 <sup>1</sup>Institute of Life Science, Swansea University Medical School, Swansea University, Swansea, SA2 8PP, UK

7 <sup>2</sup>Department of Nanomedicine, Houston Methodist Research Institute, 6670 Bertner Ave., Houston, TX  
8 77030, USA

9 <sup>3</sup>School of Pharmacy, Health Science Center, Xi'an Jiaotong University, Xi'an, Shaanxi, 710061, People's  
10 Republic of China

11 <sup>4</sup>Xi'an Jiaotong University Suzhou Academy, Suzhou 215123, People's Republic of China

12 <sup>5</sup>Ankang City Center Hospital, Ankang, Shaanxi, 725000, People's Republic of China

13  
14 \*These authors equally contributed to the work

15  
16 \*\*Corresponding author, mail: cli12@xjtu.edu.cn

17  
18 **Abstract**

19 **Background.** Amphiphilic block copolymers used as nanomicelle drug carriers can effectively overcome  
20 poor drug solubility and specificity issues. Hence, these platforms have a broad applicability in cancer  
21 treatment. In this study, Pluronic F127 was used to fabricate nanomicelles containing the histone deacetylase  
22 inhibitor SAHA, which has an epigenetic-driven anti-cancer effect in several tumor types. SAHA loaded  
23 nanomicelles were prepared using a thin-film drying method and characterized for size, surface charge, drug  
24 content and drug release properties. Loaded particles were tested for in vitro activity and their effect on cell-  
25 cycle and markers of cancer progression.

26 **Results.** Following detailed particle characterization, cell proliferation experiments demonstrated that  
27 SAHA loaded nanomicelles more effectively inhibited the growth of HeLa and MCF-7 cell lines compared  
28 with free drug formulations. The 30nm SAHA containing nanoparticles were able to release up to 100% of  
29 the encapsulated drug over a 72h time window. Moreover, gene and protein expression analyses suggested  
30 that their cytoreductive effect was achieved through the regulation of p21 and p53 expression. SAHA was  
31 also shown to upregulate E-cadherin expression, potentially influencing tumor migration.

32 **Conclusions.** This study highlights the opportunity to exploit pluronic-based nanomicelles for the delivery  
33 of compounds that regulate epigenetic processes, thus inhibiting cancer development and progression.

34  
35  
36  
37  
38  
39 **Keywords**

40 Pluronic; Drug delivery; Nanomicelles; Epigenetic drugs; Cancer; SAHA

58 **1. Background**

59

60 Chemical compounds directly targeting epigenetic processes have emerged as potential treatments for  
61 metastatic disease (Fardi et al. 2018). Epigenetics involve alterations to the DNA and chromatin landscape  
62 and consequently gene expression patterns and biological processes (Dupont et al. 2009). The molecular  
63 alterations to the nucleosome-forming histone proteins is one of the major epigenetic modifications that have  
64 been found to be altered in cancer (Audia and Campbell 2016). Compounds targeting these modifications,  
65 reverting them to a non-cancer state, have great therapeutic potential. Suberoylanilide Hydroxamic Acid  
66 (SAHA, commercially known as Vorinostat) is approved by the FDA for the treatment of malignant  
67 cutaneous T-cell lymphoma (CTCL) (Kawamata et al. 2007). Subsequently, it was found to offer therapeutic  
68 potential for other cancer types including cervical and breast (Prestegui-Martel et al. 2016; Shi et al. 2017)  
69 where female breast cancer represents around 30% of all new cancer cases in the US yearly while uterine  
70 and cervical cancer make up to 7% of the total (Siegel et al. 2020). The use of MCF-7 and HeLa for breast  
71 and cervical cancer studies involving epigenetic drugs is well established, probably due to the high genetic  
72 variability of these cells lines that could be tackled by an epigenetic approach (Landry et al. 2013; Zhou et  
73 al. 2019).

74

75 SAHA is a histone deacetylase (HDAC) inhibitor that can mediate the downregulation of DNA transcription  
76 in numerous biological processes (Haberland et al. 2009) including cell growth arrest, activation of the  
77 extrinsic and intrinsic apoptotic pathways, autophagic, reactive oxygen species (ROS)-induced cell death  
78 and mitotic cell death (Xu et al. 2007; Ververis et al. 2013; Zhang and Zhong 2014). Limitations in SAHA  
79 utility include low bioavailability, short half-life and toxic side-effects, which are partly linked to the  
80 development of multidrug resistance (MDR) (Bravo-Cordero et al. 2012; Friedl et al. 2012; Chung et al.  
81 2013). Together, these factors have limited clinical use of SAHA as an effective anticancer treatment  
82 (Konsoula and Jung 2008; Qi et al. 2017). Encapsulating SAHA within nanoparticles represents a potential  
83 strategy for overcoming such limitations to enhance its utility in clinic.

84

85 Nanoparticles including liposomes (Lee 2020), bio-nanocapsules (Tsutsui et al. 2007) and polymeric  
86 nanoparticles (El-Say and El-Sawy 2017) are being developed to overcome poor solubility and drug efficacy  
87 (Zhu and Liao 2015). Due to the unique physiological and pathological features of the tumor site, correctly  
88 sized nanomicelles can be passively targeted due to the enhanced permeability and retention (EPR) effect,  
89 which can improve the drug efficacy and reduce the toxic and side effects (Fang et al. 2011; Zhu et al. 2016;  
90 Russo et al. 2016). Nanomicelles possess unique advantages including structural stability and simplicity of  
91 fabrication in a 10-100 nm size-range (Tran et al. 2014; Kwak et al. 2015). They can also effectively prolong  
92 the retention time of drugs *in vivo* and prevent drug inactivation by enzyme degradation before reaching the  
93 tumor site (Biswas S, Vaze OS, Movassaghian S 2013).

94

95 Pluronic is a water-soluble amphiphilic molecule with a poly(oxyethylene)-block-poly (oxypropylene)-  
96 block-poly(oxyethylene) (PEOx-PPOy-PEOz) triblock structure (Farrugia et al. 2014), which self-assembles  
97 forming core-shell micelles in aqueous media. For instance, Chlorpromazine (CPZ)-containing Pluronic  
98 nanomicelles have been shown to enhance the cytotoxicity of the drug and increase its selectivity towards  
99 chronic myeloid leukemia cells, demonstrating the pharmacological potential for cancer treatment (Mello et  
100 al. 2016). Moreover, Solasodine, a type of steroidal alkaloid that exhibits excellent bioactivities against  
101 fungi, viruses, and especially tumors, has been encapsulated into Pluronic F127 nanocarriers, and was able  
102 to enhance the anti-cancer effect of Solasodine alone in A549 and Hela cells (Zhang et al. 2015). A similar  
103 approach has also been used for doxorubicin hydrochloride loaded Pluronic F127 nanocapsules which  
104 demonstrated delayed drug release (Zeng et al. 2014).

105

106 Here, we showed that the HDAC inhibitor SAHA can be efficiently loaded into pluronic F127 nanomicelles.  
107 We demonstrate that SAHA-loaded nanomicelles are able to efficiently release the drug in a time-dependent  
108 fashion. SAHA nanomicelles were shown to be more efficient than the free drug in reducing cell viability  
109 and inhibiting cell migration capacities of breast and cervical cancer cell lines, which represent two cancer  
110 types that still require more effective, epigenetic-based, treatments. Cellular uptake studies demonstrated the  
111 effective micellular uptake and intracellular distribution in a cell line dependent fashion. In addition, the free  
112 drug, the encapsulated SAHA remained effective in triggering cell cycle arrest and apoptosis in a dosage  
113 dependent manner. The histone deacetylase inhibitor drug also altered the expression of the EMT markers  
114 E-cadherin and N-cadherin suggesting that effective delivery has the potential to reverse the aggressive,

115 metastatic phenotype of these cancer models.  
116  
117  
118

## 119 2. Methods 120

### 121 2.1 Chemicals and reagents

122 Pluronic F127 was purchased from Sigma, China. SAHA was purchased from Nanjing Duolun Chemical  
123 Co., Ltd., China. Propidium Iodide (PI) was purchased from Santa Cruz Biotechnology. Acetonitrile,  
124 Dimethyl Sulfoxide (DMSO), Ammonium Persulfate, Sodium Chloride, Dodecyl Sodium Sulfate, Tween  
125 20, Methanol, Ethanol, Isopropanol and Chloroform were purchased from Sinopharm Chemical Reagent  
126 Co., Ltd., China. Phosphate Buffered Saline, Dulbecco's Modified Eagle Medium (DMEM), 1640 Medium,  
127 Trypsin were purchased from Solarbio. Fetal Bovine Serum was purchased from Corning. MTT, Glycine,  
128 Tris(hydroxymethyl)aminomethane, Acrylamide were purchased from Aladdin, China.  
129

### 130 2.2 Preparation of SAHA-Pluronic F127 Nanoparticles

131 200 mg of Pluronic F127 and 3 mg of SAHA were dissolved into 10 ml of acetonitrile. Subsequently, the  
132 solvent was removed by rotary evaporation at 55°C with decompression. The solid copolymer matrix  
133 obtained was then preheated at 65°C for 1 h and eventually hydrated with phosphate buffer solution (PBS,  
134 10mM or 150mM NaCl) or H<sub>2</sub>O. The nanomicellar solution was filtered with a 0.22 µm filter to remove any  
135 free drug. PI encapsulation was similarly achieved. 10 mg PI and 200 mg were dissolved in 10 ml of  
136 acetonitrile, and followed the same process explained above. The dispersion, size and zeta potential of  
137 nanomicelles were measured by dynamic light scattering (Particle size analyzer, Malvern, UK).  
138

### 139 2.3 Atomic Force Microscope (AFM) characterization

140 10 µL of nanomicelles aliquots were spotted on mica substrates at a concentration of 100 µg/mL (Agar  
141 Scientific, UK) and dried at room temperature. Sample topography was obtained in air using a Bruker  
142 BioScope Catalyst (Bruker Instruments, Santa Barbara, California, USA) AFM. Bruker ScanAsyst-Air  
143 cantilevers were used, with a nominal spring constant of 0.4 N/m and a nominal resonant frequency of 70  
144 kHz. All imaging was conducted using Peak Force Tapping (PFT) in ScanAsyst Mode. Images were  
145 processed with first-order flattening and planefit using Bruker Nanoscope Analysis 1.5. Gwyddion in-built  
146 grain analysis was used to identify nanomicelles and to calculate their size.  
147

### 148 2.4 Nanomicelle stability

149 Nanoparticles were resuspended in either H<sub>2</sub>O, PBS (10mM NaCl) or PBS (150 mM NaCl) and stored at  
150 4°C. In order to assess the stability of each formulation over time, size and poly-dispersion (PDI)  
151 measurements were taken at 0, 5, 10, 15, 20, 25 and 30 days.  
152

### 153 2.5 Drug release assessment

154 A high performance liquid chromatography (HPLC) system (Waters 2535, Milford, MA, US) equipped with  
155 a photodiode array detector was used for the analysis of the drug release potential of the Pluronic  
156 formulations. A C18 HPLC column (GraceSmart RP C18, 4.6 mm × 250 mm, 5 µm) was used for quantitative  
157 analysis of SAHA. Mobile phase A contained HPLC grade H<sub>2</sub>O, and mobile phase B contained HPLC grade  
158 acetonitrile. SAHA was eluted with 50% mobile phase A and mobile phase B at a flow rate of 1 ml/min, with  
159 a retention time of 3.6 min and UV detection at 265 nm. Standard curves of concentration peaks and areas  
160 were drawn. Five-point calibration curves for SAHA in the range of 31.25–500 µM were considered reliable  
161 ( $r^2 \geq 0.999$ ).  
162

### 163 2.6 Determination of drug loading and entrapment efficiency.

164 200 µl of nanomicelle solution were added with 800 µl acetonitrile and centrifuged for 5 min at 10,225 x g.  
165 The supernatant was used to determine the concentration of drug by HPLC.  
166 The entrapment efficiency (EE) and drug loading efficiency (DL) were calculated as follows:  
167

$$168 \text{DL\%} = \frac{\text{Weight of drug in nanomicelles}}{\text{Weight of drug loaded nanomicelles}} * 100\%$$

$$EE\% = \frac{\text{Weight of drug in nanomicelles}}{\text{Weight of drug added into nanomicelles}} * 100\%$$

169  
170  
171  
172  
173  
174  
175  
176  
177

## 2.7 In vitro drug release

In order to measure the release of SAHA from nanomicelles, a 20 ml solution containing SAHA loaded nanomicelles was loaded into a dialysis bag (MWCO: 8000~14,000 Da, Spectrum®, Rancho Dominguez, CA, USA), which was immersed in 500 ml of 10mM PBS (pH 7.4). Temperature was maintained at 37°C. At predetermined time intervals, 1 mL of release medium (PBS) was withdrawn and replaced with the same volume of fresh PBS into the system. The concentration of SAHA inside the solution was determined by HPLC.

178  
179

## 2.8 Cell lines

HeLa (human epithelial cervical cancer) and MCF-7 (human breast adenocarcinoma) cell lines were kindly donated by Suzhou Institute of Nano-Tech and Nano-Bionics (SINANO), Chinese Academy of Sciences. HeLa cells were grown in DMEM and MCF-7 cells in RMPI. All media was supplemented with penicillin (100 U/ml) and streptomycin (100 µg/ml) and 10% FBS at 37°C in a humidified 5% CO<sub>2</sub> and 95% air atmosphere.

185  
186

## 2.9 Cell proliferation assay

The anti-proliferative effects of SAHA, SAHA-loaded nanomicelles and empty nanomicelles were assessed using the 3-(4,5-dimethyl-2-thiazolyl)-2,5-diphenyl-2-H-tetrazolium bromide (MTT) assay (Aladdin, China). 1x10<sup>4</sup> cells/well were seeded in 96 well plates, grown overnight, and then treated with various concentrations of SAHA, SAHA loaded nanomicelles and empty nanomicelles for 24 h, 48 h or 72 h. 20 µL of MTT reagent were added to each well and left incubating for 4 hours. The optical density was determined at 490 nm using a Multifunctional Microplate Reader (Thermo Fisher, China).

193  
194

## 2.10 Protein blot

2.5x10<sup>5</sup> cells were dispersed in three 6-well plates, grown overnight, and three plates treated with SAHA, SAHA nanomicelles and empty nanomicelles for 24 h or 48 h. The cells were lysed in RIPA lysis buffer containing protease and phosphatase inhibitors (Beyotime, China) and total protein was estimated with BCA Protein Assay Kit (Beyotime, China). Protein was separated by SDS-PAGE and transferred on PVDF membranes (Beyotime, China). The membranes were blocked in 5% skimmed milk, incubated with primary antibodies for p21, p53, N-Cadherin or E-cadherin (Santac Cruz, US), and then incubated with the appropriate HRP conjugated secondary antibody (Absin, China).

202  
203

## 2.11 Quantitative RT-PCR (qRT-PCR)

Hela and MCF-7 cells were treated with the SAHA and SAHA loaded nanomicelles for 24 h or 48 h. Total RNA was isolated using the RNAiso Plus kit (Takara, Japan). 10ug of total RNA was converted into complementary DNA (cDNA) with PrimeScript RT reagent kit with gDNA Eraser (Takara, Japan). SYBR Premix Ex Taq™ II (Takara, Japan) solution was used according to manufacturer's protocol to measure for mRNA expression of p53, p21, E-cadherin and N-cadherin with by qPCR. GAPDH was used as a control to determine relative mRNA expression. The table below shows the primer sequences used.

210

Gene		Primer sequence
GAPDH	Forward Primer	5'-GCACCGTCAAGGCTGAGAAC-3'
	Reverse Primer	5'-TGGTGAAGACGCCAGTGGA-3'
p21	Forward Primer	5'-GATGGAACCTTCGACTTTGTCAACC-3'
	Reverse Primer	5'-CTGCCTCCTCCCAACTCATC-3'
p53	Forward Primer	5'-ACTCCCCTGCCCTCAACAA-3'
	Reverse Primer	5'-ATCCAAATACTCCACACGCAAA-3'
E-cadherin	Forward Primer	5'-AGGATGACACCCGGGACAAC-3'
	Reverse Primer	5'-TGCAGCTGGCTCAAGTCAAAG-3'
N-cadherin	Forward Primer	5'-CGAATGGATGAAAGACCCATCC-3'
	Reverse Primer	5'-GCCACTGCCTTCATAGTCAAACACT-3'

211  
212

## 2.12 Cellular uptake of nanomicelles

1.5x10<sup>4</sup> HeLa and MCF-7 cells/well were seeded in 8-well chambered coverslips (Ibidi). After 24 h from seeding, cells were treated with 1 μM of PI loaded Pluronic F127 nanoparticles and incubated at 37°C in a humidified atmosphere. PBS was added as the untreated control. After 4 h, 24 h and 48 h cells were washed with 1X PBS and nuclei were counterstained with Hoechst 33342 (Life Technologies). 0.1% Triton X-100 was used as a positive control and added to cells for 10 min to permeabilize them, followed by 1 μM PI treatment for 10 min. Cells were imaged live on a Zeiss LSM710 fluorescent confocal microscope (Carl Zeiss Microscopy, Jena) at a 40X magnification using the 543 nm and 405 nm laser lines.

## 2.13 Cell migration assay

MCF7 and HeLa cells were seeded at a 5x10<sup>5</sup> cells/well concentration in 6-well plates. When cells reached 90% confluence scratches were performed with a 200μl sterile pipette tip and detached cells were washed in 1X PBS. Subsequently, empty nanomicelles, SAHA-nanomicelles and free SAHA were added to each well and the final volume was brought to 2 ml with FBS-free media. Images were acquired at 0 h, 24 h and 48 h using a Zeiss inverted microscope at a 4X magnification.

Reference marks on the bottom of each well along the scratches were made to align the same fields in each image acquisition, at each time point. Image analysis of the scratches was performed using the *Wound Healing Size Tool*, an ImageJ/Fiji® plugin that allows for the quantification of the wounded area (Suarez-Arnedo et al. 2020). The scratch area was calculated for each field and time point, and the percentage of wound closure was calculated according to the following formula:

$$\text{Wound closure \%} = \left( \frac{A_{t=0} - A_{t=\Delta t}}{A_{t=0}} \right) * 100$$

Where  $A_{t=0}$  is the area of a specific field at time 0h and  $A_{t=\Delta t}$  is the area of the same field after  $n$  hours of the initial scratch. The data was graphed and analyzed using GraphPad Prism. For the statistical analysis it was used one-way ANOVA with Dunnett's multiple comparison test.

## 2.14 Statistical analysis

Data were expressed as mean ± standard deviation and analyzed using SPSS software. According to the distribution type of the data, the samples were processed by T-test and one-way ANOVA analysis with Dunnett's multiple comparison test. A pvalue P<0.05 was considered statistically significant.

## 3. Results

### 3.1 Characterization and assessment of stability of SAHA loaded nanomicelles over time

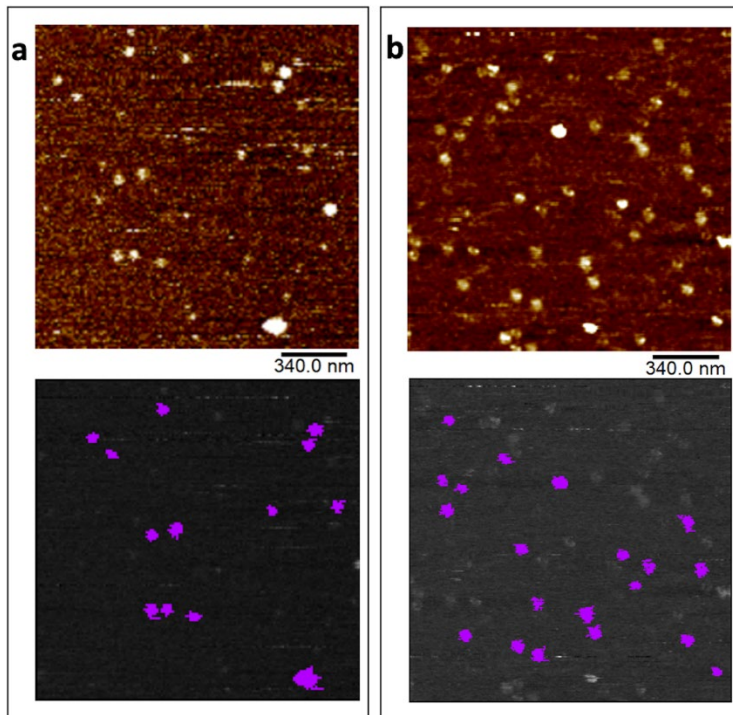
Nanomicelles were fabricated using a thin film method (see **section 2.2** materials and methods) and characterized by dynamic light scattering. Empty and SAHA loaded nanomicelles both had an average size of 23 nm and a poly-dispersive index (PDI) of 0.09±0.02 and 0.08±0.01 respectively, confirming the uniformity of distribution of the formulation (**Table 1**). The surface charge of the particles was measured with the Zetasizer Nano instrument (Malvern, UK), providing a zeta potential value of -1.28±0.28 mV. The entrapment efficiency (EE%) and Drug Loading Efficiency (DL%) values were 94.36±0.76% and 1.31±0.062%, respectively.

	Size	PDI	Zeta potential	EE%	DL%
SAHA loaded Pluronic F127 nanomicelles	22.98±1.01	0.08±0.01	-1.28±0.28	94.36±0.76	1.31±0.06
Pluronic F127 nanomicelles	22.56±0.30	0.09±0.02			

**Table 1** Characterization of SAHA encapsulated Pluronic nanomicelles. Size, PDI and surface charge were analyzed using Malvern's Zetasizer Nano. Entrapment Efficiency and Drug Loading Efficiency were calculated as explained in **Section 2.2**

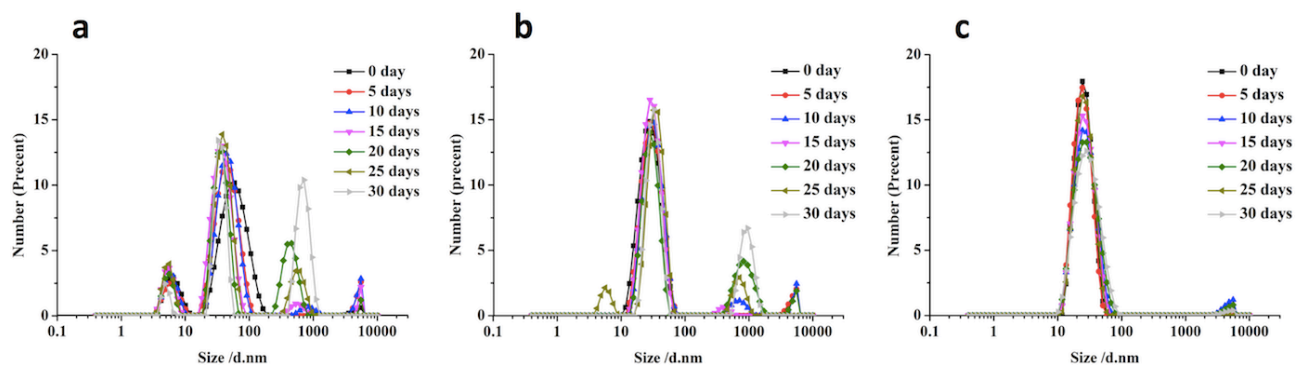
Particles were imaged using Atomic Force Microscope (AFM) and identified using the grain analysis

262 algorithm in Gwyddion (Kohn et al. 2018). Nanomicelles showed a rounded shape and both empty (**Fig. 1a**)  
 263 and SAHA-loaded (**Fig. 1b**) nanomicelles presented a diameter of 32 nm. Both AFM and DLS experiments  
 264 confirmed that no change was detectable in micelles dimensions upon incorporation of the drug.  
 265



266  
 267 **Fig. 1** AFM characterization. Empty nanomicelles and SAHA-loaded nanomicelles are shown at the top of  
 268 a and b, respectively. Z range:0-1.8 nm. Gwyddion grain analysis was used to identify nanomicelles (bottom  
 269 images, masking is highlighted in purple) and to calculate their diameter. Not all nanomicelles were  
 270 considered for grain analysis due to low masking performance.  
 271  
 272

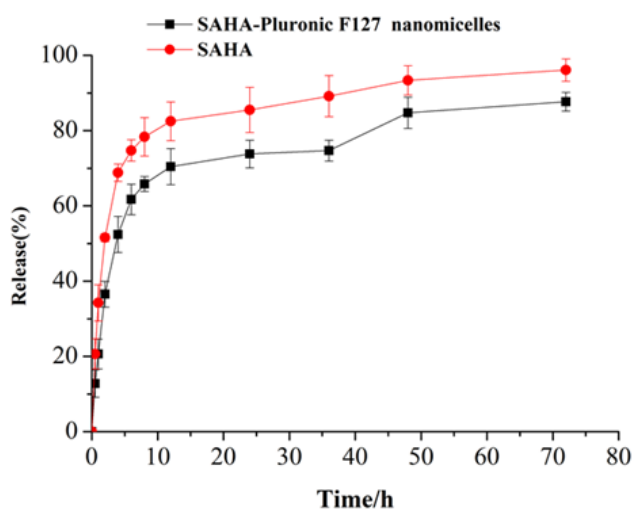
273 To determine nanomicelle stability particle size was evaluated in three different solutions (H<sub>2</sub>O, 10mM PBS  
 274 and 150mM PBS) at different time points for up to 30 days (**Fig. 2**). In all three solvents, the initial particle  
 275 size of SAHA nanomicelles was 30 nm. In H<sub>2</sub>O the micelles aggregated over time, increasing six-fold in size  
 276 compared to day 0 (**Fig. 2a**). Less aggregation was observed in 10 mM PBS (**Fig. 2b**), and no aggregation  
 277 was observed for nanomicelles dissolved in PBS containing physiological NaCl concentrations (150mM,  
 278 **Fig. 2c**). PBS (150mM NaCl) was therefore selected for all further experiments.  
 279



280  
 281 **Fig. 2** Analysis of nanoparticles stability over time. The aggregation of nanomicelles in three different solvents  
 282 was investigated at 0,5,10,15,20,25 and 30 days. Nanoparticles were kept at 4°C. **1a** H<sub>2</sub>O; **1b** 10 mM PBS; **1c** 150  
 283 mM PBS  
 284  
 285

### 286 3.2 Sustained release profiling

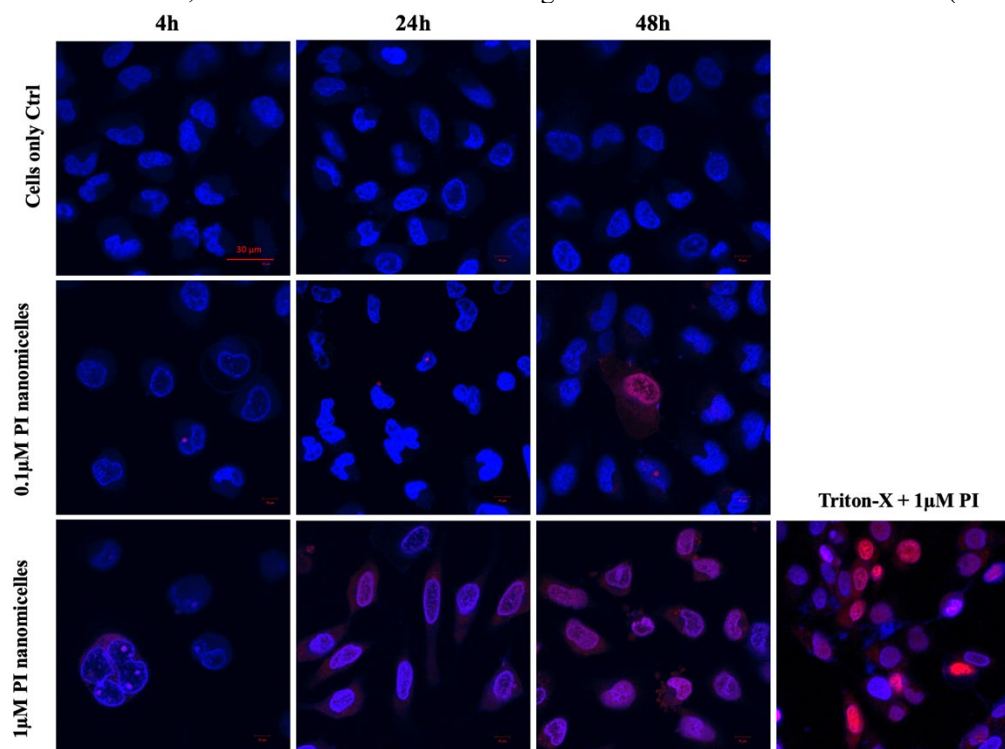
287 SAHA loaded nanomicelles were analyzed for their capacity to sustain SAHA release over time (**Fig. 3**).  
 288 SAHA was retained for a longer period of time when loaded in nanomicelles with only 36.53%  $\pm$ 3.43 of  
 289 drug released after 2 h and 85.68% $\pm$ 2.48 after 72 h, compared to free SAHA where levels reached  
 290 51.55% $\pm$ 1.56 after 2 h, 96.27%  $\pm$ 3.47 after 72 h.  
 291



292  
 293 **Fig. 3** In vitro drug release of SAHA from nanomicelles. Nanomicelles encapsulated with SAHA and  
 294 resuspended in PBS were tested for their capacity to release the drug over time. HPLC was used to measure  
 295 the amount of SAHA released after up to 72 h. The  $\pm$ SD value of the data was tested by T test (n=3).  
 296

### 297 3.3 Nanomicelles cellular uptake study

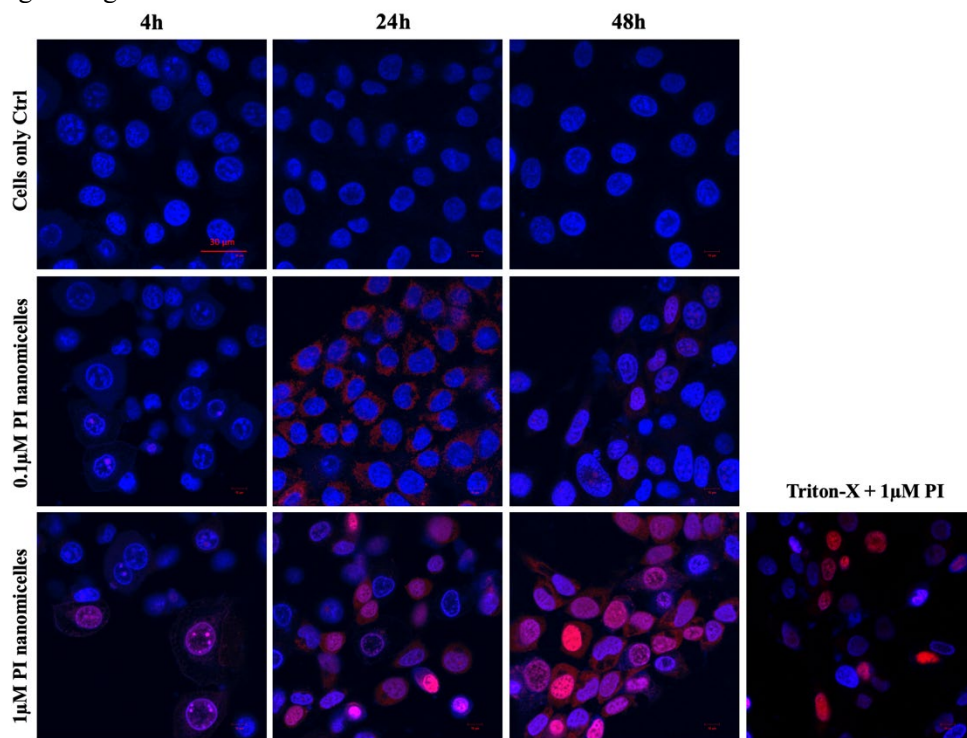
298 In order to understand the mechanisms of nanomicelles uptake HeLa and MCF-7 cells were exposed to F127  
 299 nanomicelles loaded with the fluorescent dye propidium iodide (PI). Cellular uptake was assessed at 4 h, 24  
 300 h and 48 h time points. Nanomicelle uptake by HeLa cells was measured by confocal microscopy at two  
 301 different concentrations, 0.1  $\mu$ M and 1  $\mu$ M (**Fig. 4**). Treatment with 0.1  $\mu$ M nanomicelles yielded a noticeable  
 302 PI uptake after 48 h, while the PI signal could already be visualised after 4 h following exposure to 1  $\mu$ M  
 303 PI-nanomicelles, where a clear colocalization signal was observed in the cell nuclei (blue, Fig 4).  
 304



305  
 306 **Fig. 4** PI nanomicelles uptake by HeLa cells. Confocal images were taken at 4 h, 24 h and 48 h after the

307 treatment. A negative control with unstained cells and a positive control involving the addition of Triton-X  
308 followed by PI were used. Cell nuclei are stained in blue, while PI fluorescent signal is highlighted in red.  
309  
310

311 Treatment of MCF-7 cells with PI nanomicelles resulted in a different temporal cellular uptake pattern  
312 compared to HeLa cells. Treatment with 0.1  $\mu\text{M}$  PI nanomicelles resulted in particle localization at the peri-  
313 nuclear zone after 24 h, and localization within the nuclei after 48 h, showing the intracellular transport of  
314 these particles to the nucleus can be accomplished using the delivery system. At higher treatment  
315 concentrations (1  $\mu\text{M}$ ) particles reached the cell nuclei after only 4 h from the addition and yielded the  
316 highest signal after 48 h.



317  
318 **Fig. 5 Fig. 4 PI nanomicelles uptake by MCF-7 cells.** Confocal images of MCF-7 cells were taken e at 4  
319 h, 24 h and 48 h after the treatment. A negative control with unstained cells and a positive control involving  
320 the addition of Triton-X followed by PI were used. Cell nuclei are stained in blue, while PI fluorescent signal  
321 is highlighted in red.  
322  
323

### 324 3.4 SAHA loaded nanomicelles inhibit Hela cell and MCF-7 cell proliferation

325 The ability of SAHA loaded nanomicelles to inhibit cell proliferation in both Hela and MCF-7 cancer cell  
326 lines was assessed. HeLa and MCF7 cell lines were treated with 1  $\mu\text{M}$  and 5  $\mu\text{M}$  of free drug or SAHA-  
327 encapsulated nanoparticles for up to 72 h. The 1  $\mu\text{M}$  concentration of free and encapsulated drug displayed  
328 similar toxicities with both Hela and MCF7 cells after 24 h and 48 h (**Fig. 6a, 6c**), while the nanomicelles  
329 became significantly more effective than the free drug after 72 h on HeLa cells ( $p < 0.05$ ). Conversely, the 5  
330  $\mu\text{M}$  concentration of SAHA-encapsulated nanomicelles proved to be more effective than the free drug after  
331 48 h for both HeLa ( $p < 0.05$ , **Fig. 6b**) and MCF7 ( $p < 0.01$ , **Fig. 6d**). The same trends were maintained after  
332 72 h of exposure to the treatment on both HeLa and MCF7 cells. These observations suggested that  
333 nanomicelles encapsulation of SAHA serve to enhance its cytotoxicity.  
334

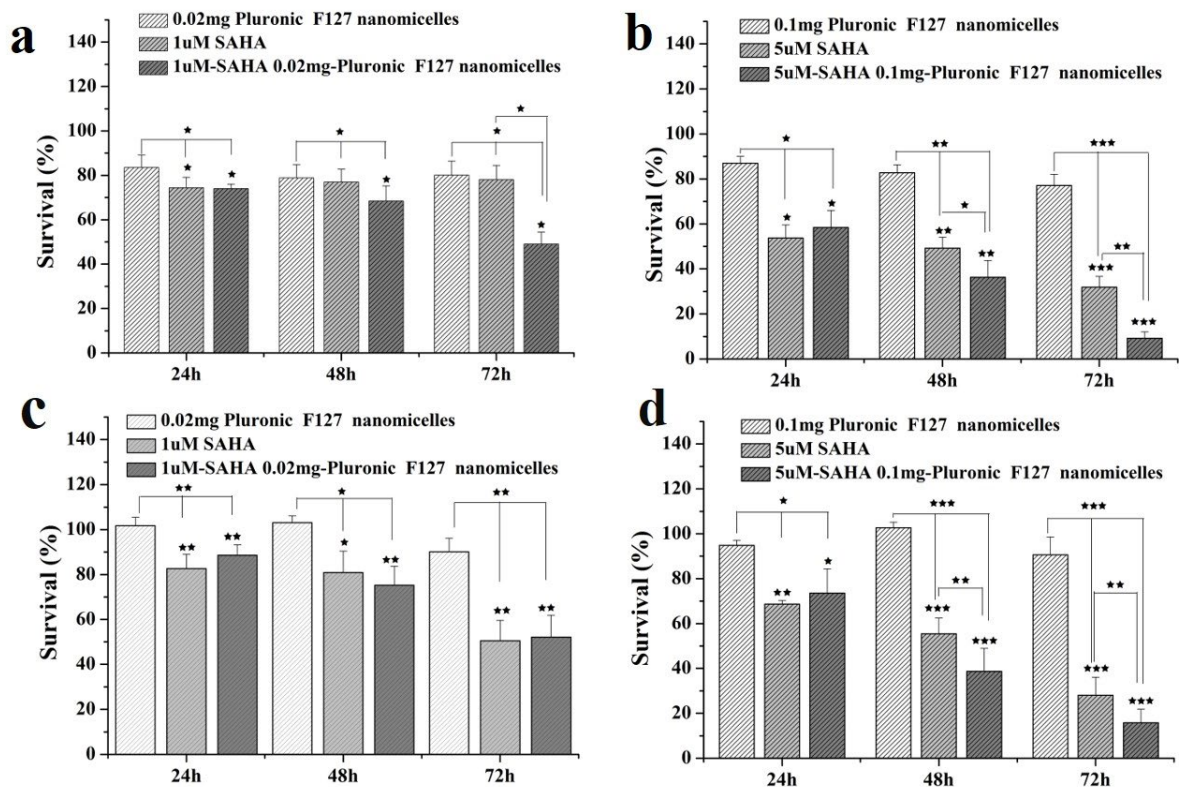
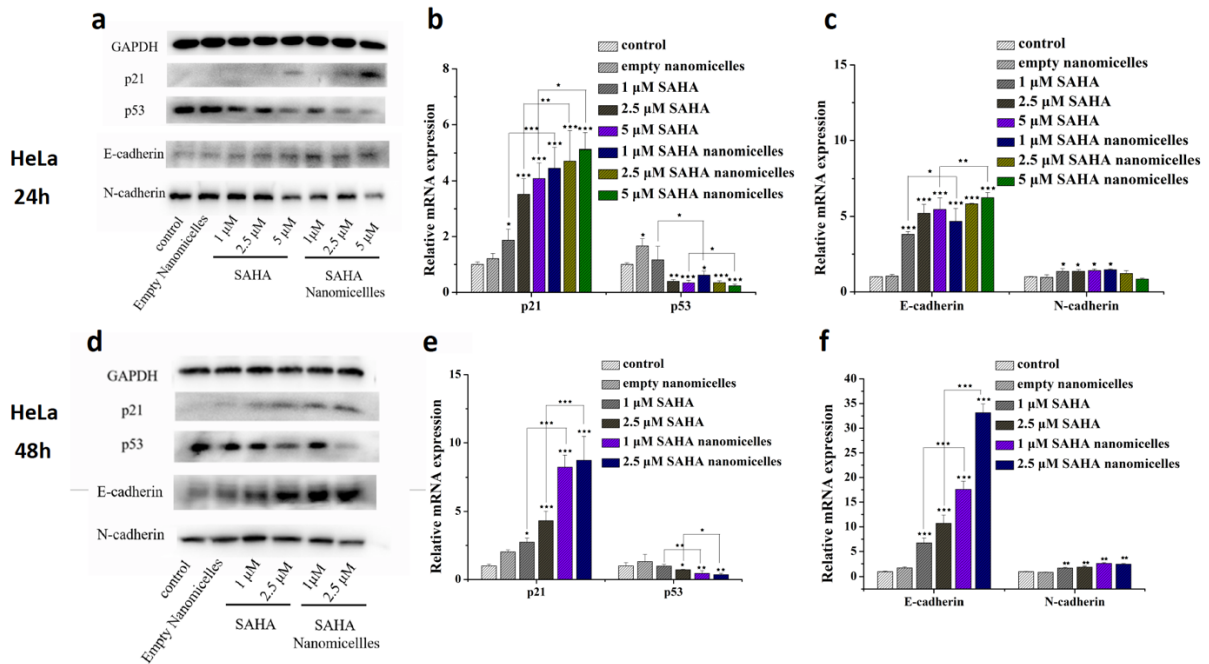


**Fig. 6** Anti-proliferative effect of SAHA on HeLa and MCF-7 cells. **6a, 6b** effect of different drug concentrations on HeLa cells at 24 h, 48 h and 72 h. **6c, 6d** effect of different drug concentrations on MCF-7 cells at 24 h, 48 h and 72 h. Survival rate was measured by MTT assay. The percentage of viable cells was determined as the ratio of treated cells to untreated controls. A one-way ANOVA was used to test for statistical significance (\* $P < 0.05$ , \*\* $P < 0.01$ , \*\*\* $P < 0.001$ ).

### 3.5 Effect of SAHA loaded nanomicelles on cell cycle and on EMT.

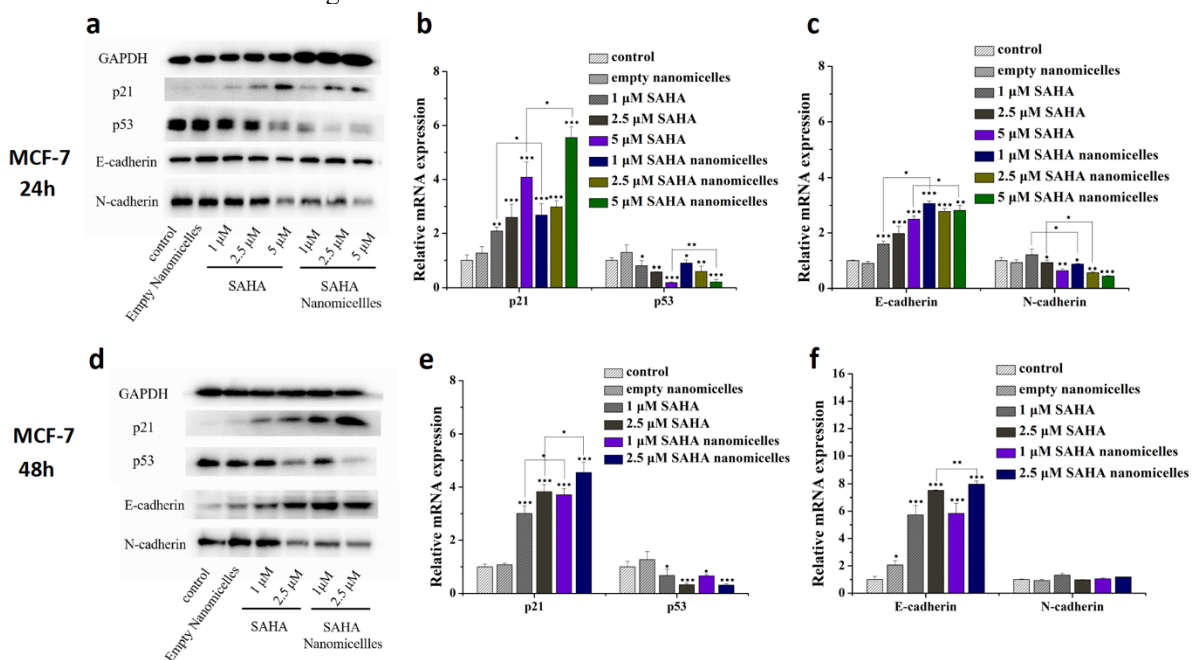
To evaluate the effect of SAHA encapsulation on the expression of p21 and p53 (cell cycle markers) and on E/N-cadherins (EMT markers), HeLa cells were treated with free and encapsulated drug for 24 h and 48 h. Increasing concentrations of both free drug and SAHA-encapsulated nanomicelles led to a significant upregulation of p21 ( $P < 0.05$ ) and a downregulation of p53 ( $P < 0.05$ ) at both 24 h (**Fig. 7a-b**) and 48 h (**Fig. 7d-e**). Moreover, SAHA loaded nanomicelles were more effective than free SAHA ( $P < 0.05$ ) in triggering alterations at the protein level (**Fig. 7a, 4b**), and this effect was corroborated by mRNA expression analysis of the same markers (**Fig. 7c, 4f**), with SAHA loaded nanomicelles having a significantly greater effect on the expression of p21 and p53 mRNA ( $P < 0.01$ ) than free drug. The effect of SAHA and SAHA-loaded nanomicelles on p21 and p53 protein expression appears concentration-dependent, with drug encapsulation potentiating the effect of SAHA in nanomicelles.

The effect of SAHA encapsulation in metastatic processes was also undertaken by determining the expression patterns of E-cadherin and N-cadherin. After 24 h, SAHA and SAHA loaded nanomicelle treatment resulted in a significant upregulation of E-cadherin protein in HeLa cells ( $P < 0.05$ ) (**Fig. 7c**). Similarly, the 48 h treatment with either SAHA and SAHA nanomicelles resulted in significantly increased E-cadherin expression ( $P < 0.05$ ) (**Fig. 7f**). SAHA-encapsulated nanoparticles were more effective than free drug in increasing E-cadherin levels. However, neither SAHA nor SAHA loaded nanomicelles had an effect on N-cadherin expression.



363  
 364 **Fig. 7** Protein and mRNA expression of p21, p53, E/N-cadherins in HeLa cells after 24 (top) or 48 hours  
 365 (bottom). Cells were analyzed by western blot and qPCR. **7a, 7d** Effect of SAHA and SAHA loaded  
 366 nanomicelles on the protein expression of the four markers in HeLa cells at 24 and 48 h. **7b, 7e** mRNA  
 367 analysis of p21 and p53 markers on HeLa cells at 24 and 48 h. **7c, 7f** Effect of SAHA and SAHA loaded  
 368 nanomicelles on E and N-cadherin mRNA expression in HeLa cells at both time points. Data were normalized  
 369 to the level of GAPDH. Data were tested by T test for statistical significance (n=3, \*P<0.05, \*\*P<0.01,  
 370 \*\*\*P<0.001).

371  
 372 The same analysis was performed on MCF-7 cells, which displayed a similar response to HeLa cells after 24  
 373 h treatment, with both SAHA and SAHA loaded micelles significantly upregulating p21 and downregulating  
 374 p53 protein (**Fig. 8a**) and mRNA expression levels (**Fig. 8b**). The same trend was seen after 48 h (**Fig. 8d-**  
 375 **e**). Furthermore, SAHA-loaded nanomicelles exhibited a greater effect on protein expression on both targets  
 376 compared to free SAHA (P<0.05). Furthermore, gene expression analysis showed a significant increase in  
 377 E- cadherin and decrease in N-cadherin after 24 h (**Fig. 8c**), which was maintained after 48 h for E-cadherin  
 378 only (**Fig. 8f**). In general, SAHA-encapsulated nanoparticles were more effective in increasing the levels of  
 379 E-cadherins than the free drug.



381 **Fig. 8** Protein and mRNA expression of p21 and p53 in MCF-7 cells after 24 (top) or 48 hours (bottom). The  
 382 effect of SAHA and SAHA loaded nanomicelles on p53 and p21 protein expression in MCF-7 cells was  
 383 analyzed. Expression of all four markers was analyzed by western blot at 24 (8a) and 48 h (8d). Data were  
 384 normalized to the level of GAPDH. The effect of SAHA and SAHA loaded nanomicelles on p21 and p53  
 385 mRNA expression was also done at 24 h (8b) and 48 h (8e), and normalized to the level of GAPDH, while  
 386 the E- and N-cadherin mRNA analysis at 24 and 48 h is shown in (8c) and (8f), respectively. The expression  
 387 level is shown relative to the control as 1. A t-test to test for statistical significance was performed (\*P<0.05,  
 388 \*\*P<0.01, \*\*\*P<0.001)

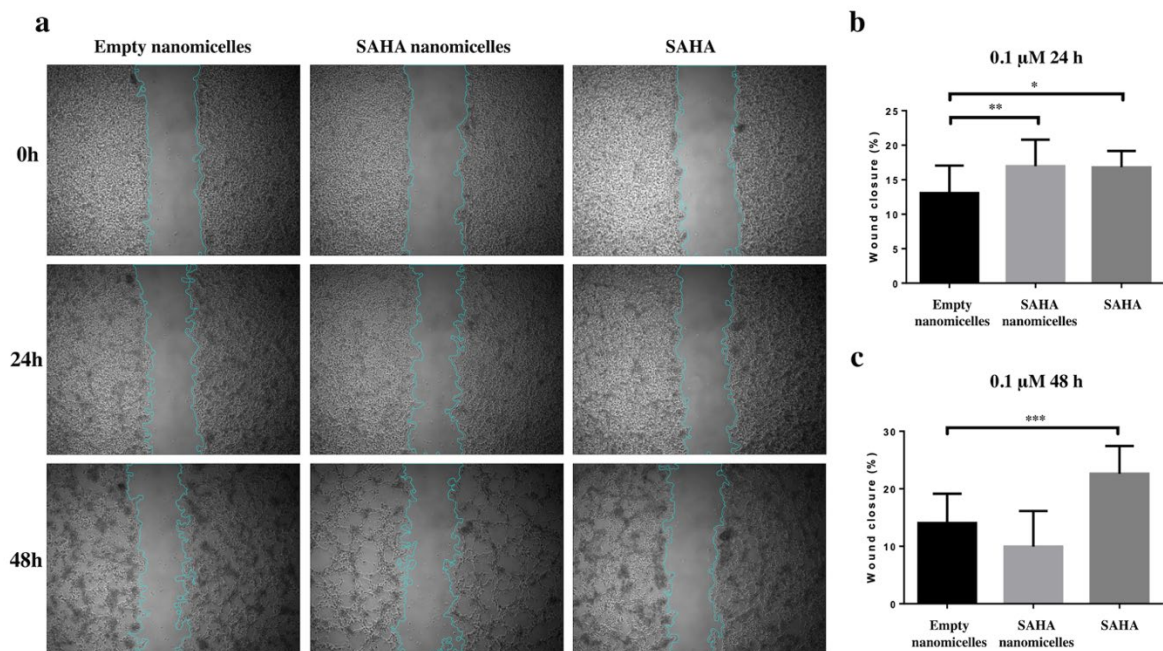
389  
 390

### 391 3.6 Analysis of cell migration capacity following SAHA nanomicelles exposure.

392 0.1  $\mu$ M SAHA nanomicelles were assessed for their ability to inhibit HeLa and MCF-7 cell growth and  
 393 migration using a wound healing assay. Following treatment for 24 h and 48 h, a time-dependent effect of  
 394 the treatment on HeLa cell division and inhibition of migration was observed (Fig. 9a). After 24 h both  
 395 SAHA-nanomicelles and SAHA were observed to inhibit wound closure compared to empty nanomicelles  
 396 ( $p<0.01$  and  $p<0.05$  respectively, Fig. 9b). After an extended 48 h treatment period the negative effect of  
 397 SAHA-nanomicelles on wound closure was more marked than the free drug, which surprisingly was even  
 398 less effective than the empty nanomicelle treatment ( $p<0.001$ , Fig. 9c).

399

400 Similarly when MCF-7 cells were exposed to 0.1  $\mu$ M SAHA nanomicelles a clear decrease in wound healing  
 401 capacity was observed after 24 h (Fig. 10a and 10b). Moreover, this effect was more enhanced after 48 h,  
 402 when SAHA-nanomicelles yielded the most marked reduction in wound closure ( $p<0.001$ ) compared to  
 403 SAHA only ( $p<0.05$ , Fig. 10c).



404

405 **Fig. 9** Effect of SAHA loaded nanomicelles on the wound closure capacity of HeLa cells . Representative  
 406 microscope images (Fig 9a) and analysis (Fig 9b) of the wound closure. Wound closure capacity values are  
 407 shown relative to the empty nanomicelles control. A one-way Anova with Dunnett's multiple comparison  
 408 test for statistical significance was performed (\*P<0.05, \*\*P<0.01, \*\*\*P<0.001)

409

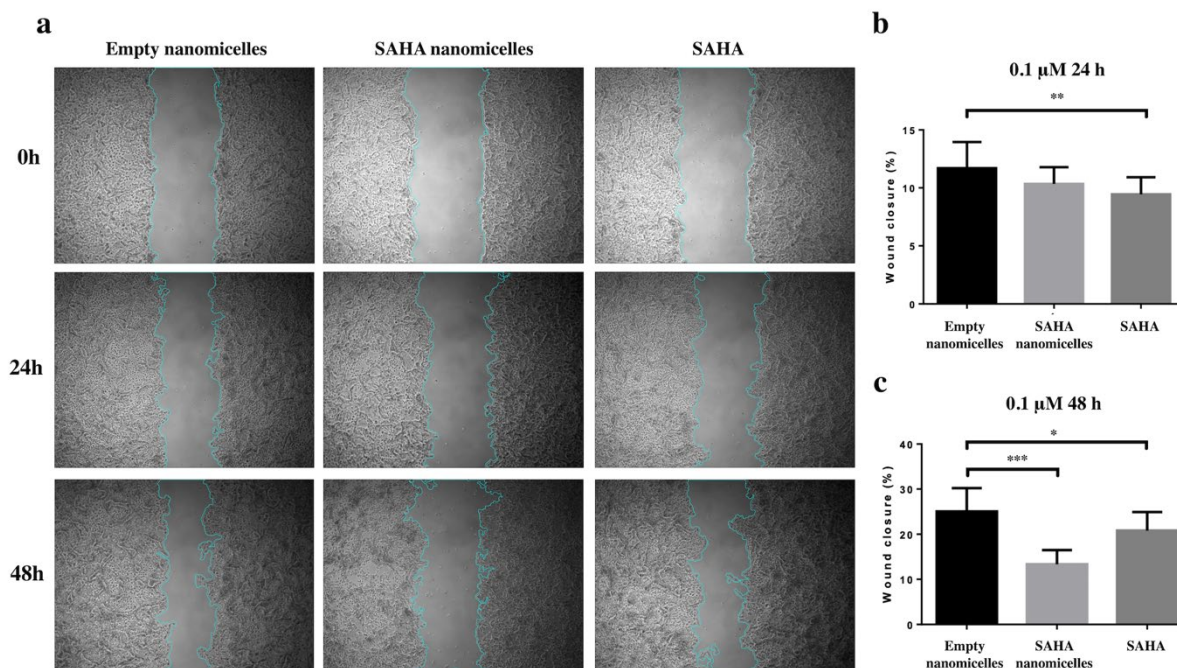


**Fig. 10** Effect of SAHA loaded nanomicelles on the wound closure capacity of MCF7 cells. Representative microscope images (Fig 10a) and analysis (Fig 10b) of the wound closure. Wound closure capacity values are shown relative to the empty nanomicelles control. A one-way Anova with Dunnett's multiple comparison test for statistical significance was performed (\* $P < 0.05$ , \*\* $P < 0.01$ , \*\*\* $P < 0.001$ )

#### 4. Discussion

Here we have demonstrated that the histone deacetylase inhibitor SAHA can be effectively encapsulated in Pluronic nanoparticles. We confirmed, by means of dynamic light scattering and AFM analysis, that the size and phenotype of nanomicelles did not change upon SAHA encapsulation.

As SAHA has been shown to cause harmful side effects, analysis of the amount of encapsulated drug within the nanomicelles was undertaken, as encapsulation could be an effective route to reducing systemic toxicity. Indeed, reported side effects include fatigue, GI related diarrhea, nausea, thrombocytopenia and anorexia as observed in different types of cancers, including endometrial cancers and lymphomas (Takai et al. 2004; Duvic 2008).

Drug release experiments showed that SAHA is progressively released from pluronic nanomicelles for up to 72h. These results were complemented by the analysis of the uptake of nanomicelles by breast and cervical cancer cell lines MCF-7 and HeLa, which showed a time-dependent nanomicelle uptake that was more enhanced in the MCF-7 cell line after 48 h. This effect could be due to different intracellular uptake patterns of nano-encapsulated formulations by different cell types. Indeed, the majority of free drugs enter the cells through a simple diffusion process, while most nanocarrier drugs enter cells through endocytosis (Kumari et al. 2016; Behzadi et al. 2017; Foroozandeh and Aziz 2018). These findings are in line with previous reports that showed the efficient employment of Pluronic F127 for the encapsulation and cellular uptake of compounds, such as curcumin (Wang et al. 2015; Vaidya et al. 2019), paclitaxel (Nie et al. 2011) and doxorubicin (Manaspon et al. 2012).

Experiments showed that nanomicelle-encapsulated SAHA was more effective than the free drug in causing cell death. This effect was most evident after 72 h, suggesting a sustained release of SAHA over time. Encapsulation could therefore result in the use of less drug while still obtaining the required therapeutic effect, or in the more effective and tumor site specific delivery due to the inherent properties of nanostructures. A wound healing assay further demonstrated the effectiveness of SAHA-nanomicelles over longer time periods for HeLa and MCF-7 cells, with a slightly different effect observed with each cell line. Indeed, the fact that breast cancer cells were more susceptible to the effect of SAHA-nanomicelles than cervical cancer cells might provide insights for future therapeutic approaches.

At the molecular level SAHA treatment caused significant changes in proteins involved in both cell cycle and cell phenotype. We demonstrated that SAHA-loaded nanomicelles were able to up-regulate p21 and

447 down-regulate p53 expression, consistent with previous studies on the action of free SAHA on tumor growth  
448 inhibition by regulating the expression of these genes (Davies et al. 2015; Ogata et al. 2017).  
449 Detailed analysis of the effects of SAHA-loaded nanoparticles on EMT transition markers revealed a  
450 significant upregulated E-cadherin expression, but with no affect N-cadherin expression. This is consistent  
451 with previous studies, where HDACi were shown to have only a slight effect on N-cadherin expression in  
452 HT-144 and A375 cells (Díaz-Núñez et al. 2016). Down-regulation or deletion of E-cadherin expression  
453 affects the cadherin-catenin complex formation and stability of the complex, which directly affects the  
454 metastatic process (Zhang et al. 2000; Guo et al. 2018). It has been suggested that SAHA may inhibit the  
455 formation of Snail and HDAC1/HDAC2 complexes by inhibiting the activity of HDAC1 and HDAC2,  
456 leading to the demethylation and transcriptional activation of the E-cadherin. In addition, SAHA may also  
457 up-regulate E-cadherin expression by altering its upstream targets (LEF-1 and Slug) (Nalls et al. 2011), but  
458 the specific mechanisms need to be further elucidated.

459

## 460 **5. Conclusions**

461 Encapsulation of SAHA into nanomicelles enhances the potency of this epigenetic drug in breast and cervical  
462 cancer cell models. Furthermore this effective formulation will likely enhance drug delivery to tumor sites,  
463 and overcome current issues in delivering HDACi to solid tumors, whilst also reducing side effects  
464 associated with systemic delivery of the free drug. The enhanced permeability and retention effect (EPR)  
465 would enable these nanoparticles to escape via neo-vascularization at tumor sites, and subsequently their  
466 physico-chemical characteristics would allow better penetration into solid tumors (Blanco et al. 2015; Zhang  
467 et al. 2019). Such parameters are likely to be specific to different cancer types, and indeed we observed that  
468 the SAHA loaded nanomicelles displayed different uptake rates, and directed intracellular trafficking in the  
469 two different cancer cell models tested here (Figs 4 & 5).

470

471

## 472 **6. Declarations**

473

474 **Competing interests.** The authors declare that they have no competing interests.

475

476 **Abbreviations.** EMT: epithelial-to-mesenchymal transition; SAHA: Suberoylanilide Hydroxamic Acid;  
477 CTCL: cutaneous T-cell lymphoma; HDAC: histone deacetylase; ROS: reactive oxygen species; TSA:  
478 trichostatin A; MDR: multidrug resistance; EPR: enhanced permeability and retention (effect); PEOx-PPOy-  
479 PEOz: poly(oxyethylene)-block-poly (oxypropylene)-block-poly(oxyethylene); CPZ: Chlorpromazine;  
480 DMSO: Dimethyl sulfoxide; DMEM: Dulbecco's Modified Eagle Medium; PBS: Phosphate buffer solution;  
481 PDI: poly-dispersion index; HPLC: High Performance Liquid Chromatography; EE: entrapment efficiency;  
482 DL: drug loading (efficiency); CDK: cyclin-dependent kinase; HDACi: Histone deacetylase inhibitors;  
483 AFM: Atomic Force Microscope; PI: Propidium Iodide.

484

485 **Authors' contributions.** Conceptualization and methodology: CL, RSC and XW; Formal analysis and data  
486 curation: SP and XW; Validation and investigation: XW, YH, LH, SP, JGP, AG and KE; Writing— original  
487 draft preparation and Writing—review and editing: SP, XW, LF, DG, CL and RSC; Approval of final  
488 manuscript: all authors. All authors read and approved the final manuscript.

489

490 **Funding.** This study received financial support from the Jiangsu Nature Science Foundation, BK20191188;  
491 the Life Sciences Research Network Wales project grant 'Nanoparticle delivery of epigenetic modifiers: a  
492 targeted approach for Endometrial Cancer treatment'; the joint PhD program Swansea University and  
493 Houston Methodist; Welsh Government ERDF SMART Expertise 2014-2020 West Wales and the Valleys  
494 Grant CEAT (Cluster for Epigenetics and Advanced Therapeutics, 2017/COL/004).

495

496 **Availability of data and materials.** The analyzed data sets generated during the present study are available  
497 from the corresponding author on reasonable request.

498

499 **Acknowledgments.** Not applicable

500

501 **Ethics approval and consent to participate.** Not applicable

502

503 **Patient consent for publication.** Not applicable

504  
505  
506  
507  
508  
509  
510  
511  
512  
513  
514  
515  
516  
517  
518  
519  
520  
521  
522  
523  
524  
525  
526  
527  
528  
529  
530  
531  
532  
533  
534  
535  
536  
537  
538  
539  
540  
541  
542  
543  
544  
545  
546  
547  
548  
549  
550  
551  
552  
553  
554  
555  
556  
557  
558  
559  
560  
561  
562  
563

## References

- Audia JE, Campbell RM (2016) Histone modifications and cancer. *Cold Spring Harb Perspect Biol.* <https://doi.org/10.1101/cshperspect.a019521>
- Behzadi S, Serpooshan V, Tao W, et al (2017) Cellular uptake of nanoparticles: Journey inside the cell. *Chem. Soc. Rev.*
- Biswas S, Vaze OS, Movassaghian S TV (2013) *Polymeric Micelles for the Delivery of Poorly Soluble Drugs.* John Wiley Sons Ltd
- Blanco E, Shen H, Ferrari M (2015) Principles of nanoparticle design for overcoming biological barriers to drug delivery. *Nat Biotechnol* 33:941–951. <https://doi.org/10.1038/nbt.3330>
- Bravo-Cordero JJ, Hodgson L, Condeelis J (2012) Directed cell invasion and migration during metastasis. *Curr. Opin. Cell Biol.*
- Chung S, Yao J, Suyama K, et al (2013) N-cadherin regulates mammary tumor cell migration through Akt3 suppression. *Oncogene.* <https://doi.org/10.1038/onc.2012.65>
- Davies C, Hogarth LA, Mackenzie KL, et al (2015) P21WAF1 modulates drug-induced apoptosis and cell cycle arrest in B-cell precursor acute lymphoblastic leukemia. *Cell Cycle.* <https://doi.org/10.1080/15384101.2015.1100774>
- Díaz-Núñez M, Díez-Torre A, De Wever O, et al (2016) Histone deacetylase inhibitors induce invasion of human melanoma cells in vitro via differential regulation of N-cadherin expression and RhoA activity. *BMC Cancer.* <https://doi.org/10.1186/s12885-016-2693-3>
- Dupont C, Armant DR, Brenner CA (2009) Epigenetics: Definition, mechanisms and clinical perspective. *Semin. Reprod. Med.* 27:351–357
- Duvic M (2008) Histone deacetylase inhibitors: SAHA (Vorinostat). A treatment option for advanced cutaneous T-cell lymphoma. *Haematol Meet Reports* 2:39–43
- El-Say KM, El-Sawy HS (2017) Polymeric nanoparticles: Promising platform for drug delivery. *Int. J. Pharm.* 528:675–691
- Fang J, Nakamura H, Maeda H (2011) The EPR effect: Unique features of tumor blood vessels for drug delivery, factors involved, and limitations and augmentation of the effect. *Adv. Drug Deliv. Rev.*
- Fardi M, Solali S, Farshdousti Hagh M (2018) Epigenetic mechanisms as a new approach in cancer treatment: An updated review. *Genes Dis.*
- Farrugia M, Morgan SP, Alexander C, Mather ML (2014) Ultrasonic monitoring of drug loaded Pluronic F127 micellular hydrogel phase behaviour. *Mater Sci Eng C.* <https://doi.org/10.1016/j.msec.2013.09.018>
- Foroozandeh P, Aziz AA (2018) Insight into Cellular Uptake and Intracellular Trafficking of Nanoparticles. *Nanoscale Res. Lett.*
- Friedl P, Locker J, Sahai E, Segall JE (2012) Classifying collective cancer cell invasion. *Nat. Cell Biol.*
- Guo M, Mu Y, Yu D, et al (2018) Comparison of the expression of TGF- $\beta$ 1, E-cadherin, N-cadherin, TP53, RB1CC1 and HIF-1 $\alpha$  in oral squamous cell carcinoma and lymph node metastases of humans and mice. *Oncol Lett.* <https://doi.org/10.3892/ol.2017.7456>
- Haberland M, Montgomery RL, Olson EN (2009) The many roles of histone deacetylases in development and physiology: Implications for disease and therapy. *Nat. Rev. Genet.*
- Kawamata N, Chen J, Koeffler HP (2007) Suberoylanilide hydroxamic acid (SAHA; vorinostat) suppresses translation of cyclin D1 in mantle cell lymphoma cells. *Blood.* <https://doi.org/10.1182/blood-2005-11-026344>
- Kohn P, Huettner S, Komber H, et al (2018) The use of the PeakForce<sup>TM</sup> quantitative nanomechanical mapping AFM-based method for high-resolution Young's modulus measurement of polymers. *Macromolecules*
- Konsoula R, Jung M (2008) In vitro plasma stability, permeability and solubility of mercaptoacetamide histone deacetylase inhibitors. *Int J Pharm.* <https://doi.org/10.1016/j.ijpharm.2008.05.001>
- Kumari P, Swami MO, Nadipalli SK, et al (2016) Curcumin Delivery by Poly(Lactide)-Based Co-Polymeric Micelles: An In Vitro Anticancer Study. *Pharm Res* 33:826–841. <https://doi.org/10.1007/s11095-015-1830-z>
- Kwak TW, Kim DH, Jeong Y Il, Kang DH (2015) Antitumor activity of vorinostat-incorporated nanoparticles against human cholangiocarcinoma cells. *J Nanobiotechnology.* <https://doi.org/10.1186/s12951-015-0122-4>

564 Landry JJM, Pyl PT, Rausch T, et al (2013) The genomic and transcriptomic landscape of a hela cell line. G3  
565 Genes, Genomes, Genet 3:1213–1224. <https://doi.org/10.1534/g3.113.005777>

566 Lee MK (2020) Liposomes for enhanced bioavailability of water-insoluble drugs: In vivo evidence and recent  
567 approaches. *Pharmaceutics* 12

568 Manaspon C, Viravaidya-Pasuwat K, Pimpha N (2012) Preparation of folate-conjugated pluronic F127/chitosan  
569 core-shell nanoparticles encapsulating doxorubicin for breast cancer treatment. *J Nanomater* 2012:.  
570 <https://doi.org/10.1155/2012/593878>

571 Mello JC de, Moraes VW, Watashi CM, et al (2016) Enhancement of chlorpromazine antitumor activity by  
572 Pluronic F127/L81 nanostructured system against human multidrug resistant leukemia. *Pharmacol Res*  
573 111:102–112. <https://doi.org/10.1016/j.phrs.2016.05.032>

574 Nalls D, Tang SN, Rodova M, et al (2011) Targeting epigenetic regulation of mir-34a for treatment of pancreatic  
575 cancer by inhibition of pancreatic cancer stem cells. *PLoS One*.  
576 <https://doi.org/10.1371/journal.pone.0024099>

577 Nie S, Hsiao WW, Pan W, Yang Z (2011) Thermoreversible pluronic® F127-based hydrogel containing liposomes  
578 for the controlled delivery of paclitaxel: In vitro drug release, cell cytotoxicity, and uptake studies. *Int J*  
579 *Nanomedicine* 6:151–166. <https://doi.org/10.2147/IJN.S15057>

580 Ogata T, Nakamura M, Sang M, et al (2017) Depletion of runt-related transcription factor 2 (RUNX2) enhances  
581 SAHA sensitivity of p53-mutated pancreatic cancer cells through the regulation of mutant p53 and TAp63.  
582 *PLoS One* 12:.  
<https://doi.org/10.1371/journal.pone.0179884>

583 Prestegui-Martel B, Bermúdez-Lugo JA, Chávez-Blanco A, et al (2016) N-(2-hydroxyphenyl)-2-  
584 propylpentanamide, a valproic acid aryl derivative designed *in silico* with improved anti-proliferative  
585 activity in HeLa, rhabdomyosarcoma and breast cancer cells. *J Enzyme Inhib Med Chem* 31:140–149.  
586 <https://doi.org/10.1080/14756366.2016.1210138>

587 Qi SS, Sun JH, Yu HH, Yu SQ (2017) Co-delivery nanoparticles of anti-cancer drugs for improving chemotherapy  
588 efficacy. *Drug Deliv*.

589 Russo A, Pellosi DS, Pagliara V, et al (2016) Biotin-targeted Pluronic ® P123/F127 mixed micelles delivering  
590 niclosamide: A repositioning strategy to treat drug-resistant lung cancer cells. *Int J Pharm* 511:127–139.  
591 <https://doi.org/10.1016/j.ijpharm.2016.06.118>

592 Shi XY, Ding W, Li TQ, et al (2017) Histone deacetylase (HDAC) inhibitor, suberoylanilide hydroxamic acid  
593 (SAHA), induces apoptosis in prostate cancer cell Lines via the Akt/FOXO3a signaling pathway. *Med Sci*  
594 *Monit* 23:5793–5802. <https://doi.org/10.12659/MSM.904597>

595 Siegel RL, Miller KD, Jemal A (2020) Cancer statistics, 2020. *CA Cancer J Clin*.  
596 <https://doi.org/10.3322/caac.21590>

597 Suarez-Arnedo A, Figueroa FT, Clavijo C, et al (2020) An image J plugin for the high throughput image analysis  
598 of in vitro scratch wound healing assays. *PLoS One* 15:.  
<https://doi.org/10.1371/journal.pone.0232565>

599 Takai N, Desmond JC, Kumagai T, et al (2004) Histone Deacetylase Inhibitors Have a Profound Antigrowth  
600 Activity in Endometrial Cancer Cells Histone Deacetylase Inhibitors Have a Profound Antigrowth Activity  
601 in Endometrial Cancer Cells. *Clin Cancer Res* 10:1141–1149

602 Tran TH, Choi JY, Ramasamy T, et al (2014) Hyaluronic acid-coated solid lipid nanoparticles for targeted delivery  
603 of vorinostat to CD44 overexpressing cancer cells. *Carbohydr Polym*.  
604 <https://doi.org/10.1016/j.carbpol.2014.08.026>

605 Tsutsui Y, Tomizawa K, Nagita M, et al (2007) Development of bionanocapsules targeting brain tumors. *J Control*  
606 *Release*. <https://doi.org/10.1016/j.jconrel.2007.06.019>

607 Vaidya FU, Sharma R, Shaikh S, et al (2019) Pluronic micelles encapsulated curcumin manifests apoptotic cell  
608 death and inhibits pro-inflammatory cytokines in human breast adenocarcinoma cells. *Cancer Rep* 2:e1133.  
609 <https://doi.org/10.1002/cnr2.1133>

610 Ververis K, Hiong A, Karagiannis TC, Licciardi P V. (2013) Histone deacetylase inhibitors (HDACIS):  
611 Multitargeted anticancer agents. *Biol. Targets Ther*.

612 Wang J, Ma W, Tu P (2015) The mechanism of self-assembled mixed micelles in improving curcumin oral  
613 absorption: In vitro and in vivo. *Colloids Surfaces B Biointerfaces* 133:108–119.  
614 <https://doi.org/10.1016/j.colsurfb.2015.05.056>

615 Xu WS, Parmigiani RB, Marks PA (2007) Histone deacetylase inhibitors: Molecular mechanisms of action.  
616 *Oncogene*

617 Zeng Z, Peng Z, Chen L, Chen Y (2014) Facile fabrication of thermally responsive Pluronic F127-based  
618 nanocapsules for controlled release of doxorubicin hydrochloride. *Colloid Polym Sci*.  
619 <https://doi.org/10.1007/s00396-014-3183-2>

620 Zhang D, Tao L, Zhao H, et al (2015) A functional drug delivery platform for targeting and imaging cancer cells  
621 based on Pluronic F127. *J Biomater Sci Polym Ed*. <https://doi.org/10.1080/09205063.2015.1030136>

622 Zhang J, Zhong Q (2014) Histone deacetylase inhibitors and cell death. *Cell. Mol. Life Sci*.

623 Zhang YR, Lin R, Li HJ, et al (2019) Strategies to improve tumor penetration of nanomedicines through

624 nanoparticle design. Wiley Interdiscip. Rev. Nanomedicine Nanobiotechnology  
625 Zhang ZY, Wu YQ, Zhang WG, et al (2000) The expression of E-cadherin-catenin complex in adenoid cystic  
626 carcinoma of salivary glands. Chin J Dent Res 3:36–9  
627 Zhou X, Liu Z, Wang H, et al (2019) SAHA (vorinostat) facilitates functional polymer-based gene transfection  
628 via upregulation of ROS and synergizes with TRAIL gene delivery for cancer therapy. J Drug Target  
629 27:306–314. <https://doi.org/10.1080/1061186X.2018.1519028>  
630 Zhu P, Zhao N, Sheng D, et al (2016) Inhibition of Growth and Metastasis of Colon Cancer by Delivering 5-  
631 Fluorouracil-loaded Pluronic P85 Copolymer Micelles. Sci Rep. <https://doi.org/10.1038/srep20896>  
632 Zhu Y, Liao L (2015) Applications of nanoparticles for anticancer drug delivery: A review. J. Nanosci.  
633 Nanotechnol. 15:4753–4773  
634  
635